A Novel Analysis Method Based on Quadratic Eigenvalue Problem for Multirelay Magnetic Coupling Wireless Power Transfer

Xinyu Hou, Yugang Su, *Member, IEEE*, Zhiping Zuo, Xin Dai, *Member, IEEE*, and Yingjun Fei

***Abstract*—To simplify the analysis process of the multirelay magnetic coupling wireless power transfer system, a novel analysis method based on the quadratic eigenvalue problem (QEP) has been proposed. The second-order underlying equation of the system is given. The eigensolution represents the inherent properties of the entire system and provides important and useful information. The analytical solutions of currents induced in each coil are expressed in terms of the eigensolution of the corresponding QEP. Real parts and imaginary parts of the eigenvalues represent attenuation coefficients and system resonance frequencies, respectively. The effect of the load resistance on the eigenvalues is studied. It is found that the attenuation coefficient of an eigenvalue increases as the load resistance increases so that it can be ignored. The relationships between eigenvalues and some key frequencies are discussed, such as system resonance frequencies, zero-phase angular frequencies, and constant voltage/current frequencies. The results show that fixed zero-phase angular frequencies and constant current frequencies are equal to the imaginary parts of the eigenvalues with load resistance is equal to zero, and the constant voltage frequencies are equal to the imaginary parts of the complex eigenvalues in a strong damping stage. Finally, experimental results verify the theoretical analysis.**

***Index Terms*—Eigensolution, eigenvalue, magnetic coupling, multirelay, quadratic eigenvalue problem, wireless power transfer.**

I. Introduction

MAGNETIC coupling wireless power transfer (MC-WPT) technology has been a research hotspot. With the advantages of safety, reliability, and flexibility, this technology has been widely used in biomedical implant equipment [1], [2], smart phones [3], electric vehicles [4], [5], and other fields. The importance of the multirelay MC-WPT system has long been a popular topic [6]. Recently, more and more attention has been paid to the analysis method and constant voltage/current characteristics of the multirelay MC-WPT system with cross-coupling [7]–[9].

For the view of analysis method, the coupled-mode theory was used to model the MC-WPT system from the energy point of view [10], [11]. The two-port network theory is used to describe the MC-WPT system to make circuit analysis of the MC-WPT system becomes simple and clear [9], [12], but relationship between system output and system parameters cannot be obtained. The ac impedance analysis method has been used to analyze the multirelay MC-WPT system [13], [14]. However, it is found that the analysis process becomes more and more complicated as the order of the system increases. The analytical transfer function and the analytical solution of the high-order system are very difficult to derive [15]. The analytical solutions of currents induced in each coil cannot be obtained. Therefore, some cross-coupling parameters and resistances of compensation network are ignored to simplify the analysis process [16], which may cause inaccurate results. A novel theoretical analysis method is proposed to reveal the general characteristic of the maximum power transfer points of MC-WPT systems in [17], but the constant voltage/current characteristic is not studied.

For the view of the constant voltage/current characteristic, the application of special circuit structures such as LCL [18] or CLC [19] compensation topologies is a common way to achieve it. Another way is to apply control method in the system. Control strategies include adding dc–dc converters [20], phase shift control [21], etc. These control strategies may require additional circuit structures. Overall, both special circuit structures and additional circuit structures increase the complexity of the system. A long-distance WPT system using domino-resonator which achieve constant current output characteristic is proposed in [22], the methodology of calculating and choosing the operating frequency in constant current mode is put forward. However, the constant voltage characteristic has not been studied.

In this article, a novel analysis method based on quadratic eigenvalue problem (QEP) has been proposed. The output characteristics of the multirelay MC-WPT system with nonnegligible cross-coupling mutual inductances and only series compensation capacitors are studied using the analysis method. The second-order underlying equation of the system is given. All system parameters are represented by only three matrices. The matrix $\boldsymbol{L}$ represents self-inductance and mutual inductance of the coupler. The matrix $\boldsymbol{R}$ represents load resistance and internal

Manuscript received November 12, 2020; revised January 22, 2021; accepted February 19, 2021. Date of publication February 26, 2021; date of current version June 1, 2021. This work was supported in part by National Key R&D Program of China by MOST under Grant 2018YFB0106300. Recommended for publication by Associate Editor J. Acero. *(Corresponding author: Yugang Su.)*

Xinyu Hou, Zhiping Zuo, Xin Dai, and Yingjun Fei are with the College of Automation, Chongqing University, Chongqing 400044, China and also with the (e-mail: 1226879853@qq.com; 564917354@qq.com; toybear@vip.sina.com; 1934563798@qq.com).

Yugang Su is with the Key Laboratory of Complex System Safety and Control, Ministry of Education, and also with the College of Automation, Chongqing University, Chongqing 400044, China (e-mail: su7558@qq.com).

Color versions of one or more figures in this article are available at https://doi.org/10.1109/TPEL.2021.3062394.

Digital Object Identifier 10.1109/TPEL.2021.3062394

resistance of the coils and capacitances. The matrix $\boldsymbol{C}$ represents compensation capacitor. The eigensolution can be obtained by solving the QEP. The relationships between eigenvalues and some key frequencies are given, such as the system resonance frequency, the zero-phase angular frequency, and the constant voltage/current frequency. The system resonant frequencies and the analytical solutions of inducted currents can be expressed in terms of the eigensolutions. The effect of the load resistance on the eigenvalues is studied, and the physical meaning of eigenvalues is explained. In the view of the multirelay MC-WPT system, this article focuses on the following:

1) Simplification of the analysis process without ignoring system parameters.
2) Constant voltage/current characteristics without special topologies and control methods.

This article has been organized as follows. Section II presents the analysis method for the multirelay MC-WPT system with series compensation capacitors and explains the physical meaning of eigenvalues. Followed by Section III, the effect of load resistance on the eigenvalue is studied, and the relationships between eigenvalues and some key frequencies are discussed. In Section IV, the simulation model and the prototype are built to validate the feasibility of theoretical analysis. Finally, Section V concludes this article.

II. Analysis Method Based on Quadratic Eigenvalue Problem

A. System Description

Fig. 1 shows the circuit of a *n*-coil multirelay MC-WPT system with only series compensation capacitors. The *n* coils and *n* capacitors compose the coupler, and each coil is in series with a capacitor to form an oscillating circuit. Variables with the subscript *m* represents the parameters in the *k*th oscillating circuit ($k = 1, 2,..., n$). L_k represents self-inductance of the *k*th coil. M_{ij} represents the mutual inductance between the *i*th coil and the *j*th coil ($M_{ij} = M_{ji}$). C_k represents the compensating capacitance of the *k*th circuit. R_k represents the sum of the equivalent series resistance (ESR) of L_k and C_k. R_{L} represents the load resistance. The dc supply is represented by V. S_1, S_2, S_3, and S_4 denote the full-bridge inverter. D_1, D_2, D_3, and D_4 donote rectifier. C_{L} represents the filter capacitor. $u(t)$ represents the dc voltage supply as a function of time and can be expressed as

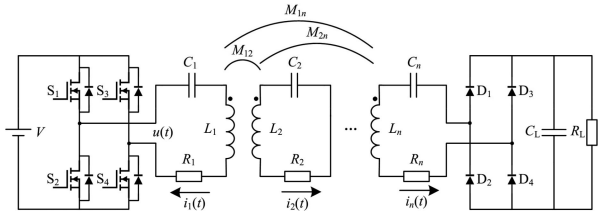

Fig. 1. Circuit of a *n*-coil multirelay MC-WPT system.

$$u(t) = \begin{cases} V & t \in [0, \frac{T}{2}) \\ -V & t \in [\frac{T}{2}, T) \end{cases} \tag{1}$$

where T is the period.

Obviously, $u(t)$ meet the Dirichlet condition. Therefore, it can be decomposed into the form of Fourier infinite series, as shown in (2). ω is the supply angular frequency. Because of the good low-pass filtering characteristics of the multirelay MC-WPT system, the high order harmonics can be effectively eliminated, $u(t)$ can be transformed into (3). The expression of the equivalent load resistance R_{Leq} is shown as (4)

$$u(t) = \frac{4V}{\pi} \sum_{k=0}^{n} \sin\left((2k-1)\,\omega t\right) \tag{2}$$

$$u(t) \approx \frac{4V}{\pi} \sin(\omega t) \tag{3}$$

$$R_{Leq} = \frac{8}{\pi^2} R_L. \tag{4}$$

B. System Modeling

The equivalent circuit of a *n*-coil multirelay MC-WPT system is shown in Fig. 2. According to Kirchhoff's voltages law, the system equation of the *n*-coil multirelay MC-WPT system can

$$\begin{cases} L_1 \frac{di_1(t)}{dt} + M_{12} \frac{di_2(t)}{dt} + \cdots + M_{1n} \frac{di_n(t)}{dt} + R_1 i_1(t) + \frac{1}{C_1} q_1(t) = u(t) \\ M_{21} \frac{di_1(t)}{dt} + L_2 \frac{di_2(t)}{dt} + \cdots + M_{2n} \frac{di_n(t)}{dt} + R_2 i_2(t) + \frac{1}{C_2} q_2(t) = 0 \\ \vdots \\ M_{n1} \frac{di_1(t)}{dt} + M_{n2} \frac{di_2(t)}{dt} + \cdots + L_n \frac{di_n(t)}{dt} + (R_n + R_{\mathrm{Leq}})\, i_n(t) + \frac{1}{C_n} q_n(t) = 0 \end{cases} \tag{5}$$

$$\begin{cases} L_1 \frac{d^2 i_1(t)}{dt^2} + M_{12} \frac{d^2 i_2(t)}{dt^2} + \cdots + M_{1n} \frac{d^2 i_n(t)}{dt^2} + R_1 \frac{di_1(t)}{dt} + \frac{1}{C_1} i_1(t) = \frac{du(t)}{dt} \\ M_{21} \frac{d^2 i_1(t)}{dt^2} + L_2 \frac{d^2 i_2(t)}{dt^2} + \cdots + M_{2n} \frac{d^2 i_n(t)}{dt^2} + R_2 \frac{di_2(t)}{dt} + \frac{1}{C_2} i_2(t) = 0 \\ \vdots \\ M_{n1} \frac{d^2 i_1(t)}{dt^2} + M_{n2} \frac{d^2 i_2(t)}{dt^2} + \cdots + L_n \frac{d^2 i_n(t)}{dt^2} + (R_n + R_{\mathrm{Leq}}) \frac{di_n(t)}{dt} + \frac{1}{C_n} i_n(t) = 0. \end{cases} \tag{7}$$

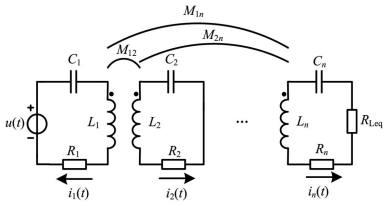

Fig. 2. Equivalent circuit of a *n*-coil multirelay MC-WPT system.

be expressed as (6) where q_k(t) is the charge on the capacitor C_k, i_k(t) is the current through the coils, and t is the elapsed time.

The charge q_k (t) is related to the current i_k (t) by

$$i_k(t) = \frac{dq_k(t)}{dt}. \tag{6}$$

Differentiation of (5), shown at the bottom of the previous page, gives the second-order differential equation of the system in (7), shown at the bottom of the previous page

This article separately defines the matrix $\boldsymbol{L}$, the matrix $\boldsymbol{R}$, the matrix $\boldsymbol{C}$ as

$$\mathbf{L} = \begin{bmatrix} L_1 & M_{12} & \cdots & M_{1n} \\ M_{21} & L_2 & \cdots & M_{2n} \\ \vdots & \vdots & \ddots & \vdots \\ M_{n1} & M_{n2} & \cdots & L_n \end{bmatrix} \tag{8}$$

$$\mathbf{R} = \begin{bmatrix} R_1 & 0 & \cdots & 0 \\ 0 & R_2 & \cdots & 0 \\ \vdots & \vdots & \ddots & \vdots \\ 0 & 0 & \cdots & R_n + R_{\text{Leq}} \end{bmatrix} \tag{9}$$

$$\mathbf{C} = \begin{bmatrix} {C_1}^{-1} & 0 & \cdots & 0 \\ 0 & {C_2}^{-1} & \cdots & 0 \\ \vdots & \vdots & \ddots & \vdots \\ 0 & 0 & \cdots & {C_n}^{-1} \end{bmatrix}. \tag{10}$$

The underlying equation of the system expressed by the above three matrixes is as follows:

$$\mathbf{L}\frac{d^2\mathbf{i}(t)}{dt^2} + \mathbf{R}\frac{d\mathbf{i}(t)}{dt} + \mathbf{C}\mathbf{i}(t) = \mathbf{f}(t) \tag{11}$$

where $\boldsymbol{L}$, $\boldsymbol{R}$, and $\boldsymbol{C}$ are $n\times n$ matrices, $\boldsymbol{i}$(t) and $\boldsymbol{f}$(t) are the nth order vectors, $\boldsymbol{i}(t) = [\, i_1(t)\ i_2\ (t)\ \cdots\ i_{\text{n}}(t)]^T$, and $\boldsymbol{f}$ (t) = [d$u(t)$/dt $0\ \cdots\ 0]^T$, respectively.

There is only one supply in the system. In this case, the model of the system can be expressed as (12). $p(t)$ represents the differential of supply voltage. $\boldsymbol{y}(t)$ represents the output current. $\boldsymbol{H}$ and $\boldsymbol{D}$ are selection matrixes. Elements in $\boldsymbol{D}$ depend on practices

$$\begin{cases} \mathbf{L}\frac{d^2\mathbf{i}(t)}{dt^2} + \mathbf{R}\frac{d\mathbf{i}(t)}{dt} + \mathbf{C}\mathbf{i}(t) = \mathbf{H}p\,(t) \\ \mathbf{y}\,(t) = \mathbf{D}\mathbf{i}(t) \end{cases} \tag{12}$$

$$\mathbf{H} = \begin{bmatrix} 1\ 0\ \cdots\ 0 \end{bmatrix}^T \tag{13}$$

$$p(t) = \frac{du(t)}{dt}. \tag{14}$$

C. Eigensolution of the System

Equation (15) is an $n \times n$ matrix polynomial of degree 2, the coefficients of the matrix $\boldsymbol{Q}(\lambda)$ are quadratic polynomials in the scalar λ. Matrix $\boldsymbol{Q}(\lambda)$ is often called λ-matrix

$$\mathbf{Q}\,(\lambda) = \lambda^2\mathbf{L} + \lambda\mathbf{R} + \mathbf{C}. \tag{15}$$

The spectrum of $\boldsymbol{Q}(\lambda)$ is denoted by $\Lambda(\boldsymbol{Q})$, it is the set of the eigenvalues of $\boldsymbol{Q}(\lambda)$

$$\begin{aligned} \Lambda\,(\mathbf{Q}) &= \{\lambda \in \mathbb{C} : \det \mathbf{Q}\,(\lambda) = 0\} \\ &= \operatorname{diag}\,(\lambda_1, \lambda_2, \ldots, \lambda_{2\text{n}}) \end{aligned} \tag{16}$$

where diag(λ_1, λ_2, …, λ_{2n}) represents the diagonal matrix with λ_1, λ_2, …,$\lambda_{2\,n}$ as elements.

Let $\boldsymbol{X}$ and $\boldsymbol{Y}$ represent eigenvectors of the $\boldsymbol{Q}(\lambda)$; $\boldsymbol{x}_i$ and $\boldsymbol{y}_i$ are right and left eigenvectors, respectively, corresponding to λ_i

$$\begin{aligned} \mathbf{X} &= [\mathbf{x}_1, \mathbf{x}_2, \ldots, \mathbf{x}_{2n}] \\ \mathbf{Y} &= [\mathbf{y}_1, \mathbf{y}_2, \ldots, \mathbf{y}_{2n}]\,. \end{aligned} \tag{17}$$

To get the eigensolution, $\boldsymbol{Q}(\lambda)$ of degree 2 is reduced to the first-order equation. It is transformed into the form of $\boldsymbol{Ax}$ - $\lambda\boldsymbol{Bx} = 0$. Most of the reductions used in practice are of the companion form 1 and the companion form 2

$$\begin{aligned} \text{form}\,1 &: \begin{bmatrix} \mathbf{0}^{n\times n} & \mathbf{N} \\ -\mathbf{C} & -\mathbf{R} \end{bmatrix}\mathbf{x} - \lambda\begin{bmatrix} \mathbf{N} & \mathbf{0}^{n\times n} \\ \mathbf{0}^{n\times n} & \mathbf{L} \end{bmatrix}\mathbf{x} = 0 \\ \text{form}\,2 &: \begin{bmatrix} -\mathbf{C} & \mathbf{0}^{n\times n} \\ \mathbf{0}^{n\times n} & -\mathbf{R} \end{bmatrix}\mathbf{x} - \lambda\begin{bmatrix} \mathbf{R} & \mathbf{L} \\ \mathbf{N} & \mathbf{0}^{n\times n} \end{bmatrix}\mathbf{x} = 0 \end{aligned} \tag{18}$$

where $\boldsymbol{0}^{n\times n}$ represents the $n\times n$ null matrix, and $\boldsymbol{N}$ can be any nonsingular $n\times n$ matrix.

After the reduction, generalized eigenvalue and the generalized eigenvector of the pair ($\boldsymbol{A}$, $\boldsymbol{B}$) can be obtained by computing the generalized Schur decomposition.

D. Induced Currents and Resonance Frequencies

Resonance frequencies of the multirelay MC-WPT system are determined by the coupler and the load, and it is independent of the supply. The resonant frequency can be obtained by solving the eigenvalues of the QEP. In the n-coil multirelay MC-WPT systems, $\boldsymbol{L}$, $\boldsymbol{R}$, and $\boldsymbol{C}$ are real symmetric positive definite, so all eigenvalues are real or come in pairs (λ,λ^*) [23]. Therefore, only part of them needs to be considered during the analysis. This article only analyzes the eigenvalues above the real axis. $\boldsymbol{L}$ is a diagonally dominant matrix in general, so it is nonsingular. When $\boldsymbol{L}$ is nonsingular, there are $2n$ finite eigenvalue. The real part Re(λ_k) of λ_k is the attenuation coefficient, and imaginary part Im(λ_k) of λ_k is approximately equal to the system resonance frequency. In general, there are n system resonance frequencies in the n-coil multirelay MC-WPT systems.

When $\boldsymbol{L}$ is nonsingular and all the eigenvalues are simple, the general and special solutions of the homogeneous differential equation are shown in (19) and (20), and they form the solution of the homogeneous differential equation together as shown in (21). $\boldsymbol{a}$ is a constant vector and is related to the initial state, as shown in (22). The special solution $\boldsymbol{i}_p(t)$ decrease exponentially

to zero as $t\to\infty$, so the steady-state induced current is equal to the general solution $\boldsymbol{i}_g$(t)

$$i_g(t)=\sum_{k=1}^{2n}a_k\mathbf{x}_k e^{\lambda_k t}=\mathbf{X}e^{\Lambda t}\mathbf{a} \tag{19}$$

$$\mathbf{i}_p(t)=\mathbf{X}e^{\Lambda t}\int_0^t e^{-\Lambda s}\mathbf{Y}\mathbf{H}p(s)ds \tag{20}$$

$$\mathbf{i}(t)=\mathbf{i}_g(t)+\mathbf{i}_p(t)=\mathbf{X}e^{\Lambda t}\left(\alpha+\int_0^t e^{-\Lambda s}\mathbf{Y}\mathbf{H}p(s)ds\right) \tag{21}$$

$$\alpha=[a_1,\ldots,a_{2n}]^T. \tag{22}$$

Calculation formula of matrix function $e^{\Lambda t}$ is

$$e^{\Lambda t}=\sum_{k=1}^{+\infty}\frac{1}{k!}\Lambda^k t^k. \tag{23}$$

Because Λ is a diagonal matrix, by transforming (23), we have

$$e^{\Lambda t}=diag\left(\sum_{k=0}^{+\infty}\tfrac{1}{k!}{\lambda_1}^k t^k\ \sum_{k=0}^{+\infty}\tfrac{1}{k!}{\lambda_2}^k t^k\ \cdots\ \sum_{k=0}^{+\infty}\tfrac{1}{k!}{\lambda_n}^k t^k\right). \tag{24}$$

Combined (24) and the power series expansion of the exponential function, $e^{\Lambda t}$ and $e^{-\Lambda s}$ can be calculated by

$$e^{\Lambda t}=\mathrm{diag}\left(e^{\lambda_1 t}\ e^{\lambda_2 t}\ \cdots\ e^{\lambda_n t}\right) \tag{25}$$

$$e^{-\Lambda s}=\mathrm{diag}\left(e^{-\lambda_1 s}\ e^{-\lambda_2 s}\ \cdots\ e^{-\lambda_n s}\right). \tag{26}$$

Thus, we transform (21) into

$$\mathbf{i}(t)=\sum_{k=1}^{2n}\frac{\mathbf{x}_k\mathbf{y}_k^*}{i\omega-\lambda_k}\mathbf{H}p(t) \tag{27}$$

where ω is the angular frequency of the supply voltage and $\boldsymbol{y}^*$ represents the conjugate transpose of $\boldsymbol{y}$.

Taking Laplace transforms of (27), we can obtain the system transfer function $G(s)$ as

$$G(s)=\mathbf{D}\mathbf{X}(s\mathbf{E}-\Lambda)^{-1}\mathbf{Y}^*\mathbf{H} \tag{28}$$

where $\boldsymbol{E}$ represents the $n$thorder identity matrix and $\boldsymbol{Y}^*$ represents the conjugate transpose of $\boldsymbol{Y}$.

The expressions of the equivalent system transfer impedance Z and output current gain K are shown as

$$Z=\frac{1}{sG(s)},\quad \mathbf{D}=\left[1\ 0\ \ldots\ 0\right] \tag{29}$$

$$K=\frac{1}{sG(s)},\quad \mathbf{D}=\left[0\ 0\ \ldots\ 1\right]. \tag{30}$$

The analytical solutions of the system resonance frequencies and the zero-phase angular frequencies can be expressed in terms of the eigenvalues and eigenvectors of the system. The zero-phase angular frequencies are represented by ω_Z, which is shown as (31). The resonance of MC-WPT systems refers to the sharp increase of the current amplitudes of the system, the operating frequencies for the maximum current amplitudes are defined as the system resonant frequencies of the MC-WPT system [24].

According to (27), the induced current reaches a local maximum value when $i\omega$ is equal to Im(λ_k). Therefore, the system resonance frequencies are approximately equal to the imaginary part of the eigenvalues, and the expression of the system resonance frequency ω_S is shown as

$$\omega_Z=\left\{\omega\in\mathbb{R}:\mathrm{Im}\left(D\sum_{k=1}^{2n}\frac{\mathbf{x}_k\mathbf{y}_k^*}{i\omega-\lambda_k}H\right)=0\right\}$$

$$D=\left[1\ \cdots\ 0\ 0\right] \tag{31}$$

$$\omega_S=\left\{\omega\in\mathbb{R}:\omega\approx\mathrm{Im}\left(\lambda_k\right),k=1:2n\right\}. \tag{32}$$

TABLE I
SYSTEM PARAMETERS OF SIMULATION MODEL

Parameter	Value	Parameter	Value
number of turns	10	transmission distance d	50 mm
layers of the coil	1	wire diameter	2 mm
radii of the coil	100 mm	supply voltage V	24V
Inductance $L_1\ldots L_n$	31.92 uH	Capacitance $C_1\ldots C_n$	19.84 nF
ESR $R_1\ldots R_n$	30 mΩ		

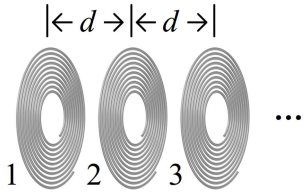

Fig. 3. Multirelay MC-WPT system. The normal lines of all coils are in the same direction, and the transmission distance d between adjacent coils is the same.

III. Relationship Between Key Frequencies and Eigenvalues

The multirelay MC-WPT system parameters are shown in Table I [17]. The methodology of the relationship between key frequencies and eigenvalues is demonstrated with the use of a multirelay MC-WPT system, as shown in Fig. 3. This article employs Neumann's equation to calculate M between these two coils [25], and Fig. 4 shows the curve of mutual inductance M with the distance d between these two concentric coils.

It should be noted that most multirelay MC-WPT systems are used when the parameters of the coupler are fixed [14], [18], [22]. The coils of the system in this article are arranged in a fixed distance. The mutual inductances of different pairs of coils are equal ($M_{12}=M_{23}=\ldots, M_{13}=M_{24}=\ldots$).

A. Variation of Eigenvalues With Load Resistance

According to (27), the system output is closely related to eigenvalues. Therefore, the variation of eigenvalues with load resistance is analyzed first. Eigenvalues associate load resistance with system output. MATLAB is used to simulate the multirelay MC-WPT systems. In the 3-coil MC-WPT system, the variation

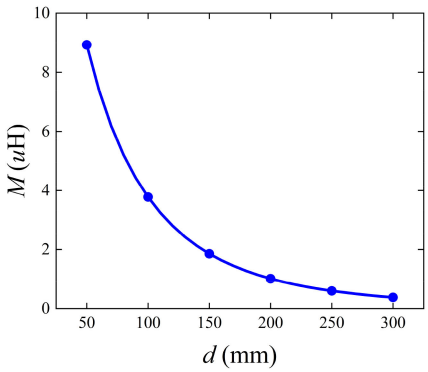

Fig. 4. Curve of mutual inductance M with transmission distance d.

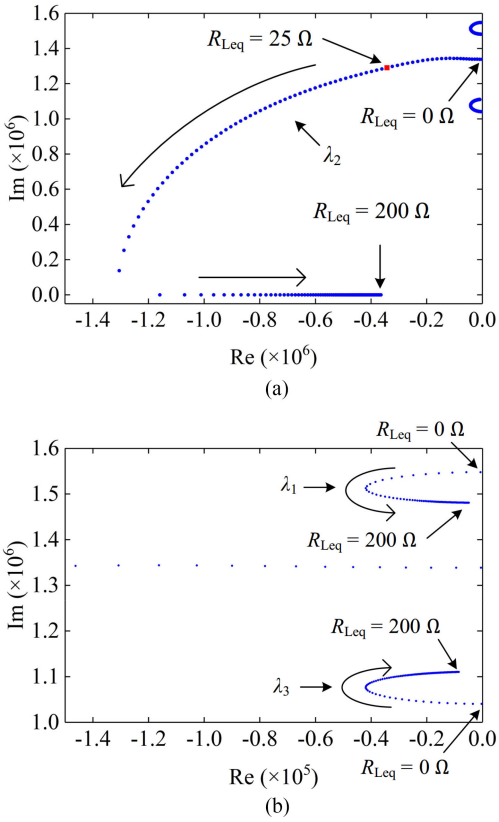

Fig. 5. Variation of the eigenvalues with the equivalent load resistance R_{Leq} in the 3-coil MC-WPT system: (a) global eigenvalues; and (b) partial eigenvalues.

of the eigenvalues with the equivalent load resistance R_{Leq} is shown in Fig. 5 according to (16). The horizontal axis is the real axis and the vertical axis is the imaginary axis. Since the eigenvalues are complex conjugates in pairs, only the eigenvalues above the real axis are given. As R_{Leq} increases, three eigenvalues change in the direction shown by the arrow in Fig. 4. When R_{Leq} exceeds 25 Ω, $\mathrm{Re}(\lambda_2)$ is much higher than $\mathrm{Re}(\lambda_1)$ and $\mathrm{Re}(\lambda_3)$. Hence, it can be obtained from (27) that the induced currents only be related to λ_1 and λ_3. As R_{Leq} increases, $\mathrm{Re}(\lambda_1)$ and $\mathrm{Re}(\lambda_3)$ increase first and then decrease, $\mathrm{Im}(\lambda_1)$ gradually decreases, and $\mathrm{Im}(\lambda_2)$ gradually increases. As R_{Leq} increases to

TABLE II
COMPARISON OF EIGENVALUES, ZERO-PHASE ANGULAR FREQUENCIES, AND SYSTEM RESONANCE FREQUENCIES OF THE 3-COIL MC-WPT SYSTEM

R_{Leq}	λ (×10^6)	ω_S (×10^6)	ω_Z (×10^6)
5Ω	-0.0155 ± 1.0428i -0.0465 ± 1.3399i -0.0248 ± 1.5410i	1.0443 1.3439 1.5363	1.0486 1.1107 1.3496 1.4815 1.5220
14Ω	-0.0368 ± 1.0592i -0.1624 ± 1.3409i -0.0407 ± 1.5047i	1.0677 1.4948	1.4802
50Ω	-0.8155 ± 1.0325i -0.0241 ± 1.1048i -0.0133 ± 1.4821i	1.1067 1.4815	1.1109 1.2483 1.4806
150Ω	-0.0085 ± 1.1102i -0.0049 ± 1.4809i -4.7209 -0.3639	1.1104 1.4808	1.1109 1.2558 1.4807

greater than 148 Ω, $\mathrm{Im}(\lambda_2)$ decreases to 0. At this time, there are two resonance frequencies in the system, which is equivalent to a short circuit on load resistance in the 2-coil MC-WPT system. If the load resistance is too large, the matrix R will be ill-conditioned, which may cause the condition number of the eigenvalue calculation to increase [26]. However, the open circuit at load resistance is not allowed during operation, so it can be avoided.

When R_{Leq} is 5, 14, 50, and 148 Ω, eigenvalues, zero-phase angular frequencies, and system resonant frequencies of the *3*-coil MC-WPT system are calculated as shown in Table II according to (16), (31), and (32). When R_{Leq} is 5 Ω, $\mathrm{Re}(\lambda_1)$, $\mathrm{Re}(\lambda_2)$, and $\mathrm{Re}(\lambda_3)$ are all small, there are three system resonance frequencies. As $\mathrm{Re}(\lambda_2)$ gradually increases, the number of the system resonances frequencies decreases to two. The system resonance frequencies slightly shift, because three resonance modes interact with each other. As for the zero-phase angle frequency, 1.48 × 10^6 rad/s is fixed in each of four equivalent load resistances.

B. Zero-Phase Angle Frequencies

According to (31), input phase angular θ versus the supply angular frequency ω of the 3-coil MC-WPT system is shown in Fig. 6. Two fixed zero-phase angle frequencies highlighted with dotted round frames. When R_{Leq} is 14 Ω, phase angular in 1.11 × 10^6 rad/s is very small. Hence, 1.11 × 10^6 rad/s can be approximated as zero-phase angle frequency too.

In order to study the relationship between the eigenvalues and the zero-phase angular frequency with different load resistance, the input phase angle θ versus the supply angular frequency ω and equivalent load resistance R_{Leq} of the 3-coil MC-WPT system is shown in Fig. 7 according to (16) and (31). The horizontal axis represents R_{Leq}, the vertical axis represents the supply angular frequency ω, the black dotted line represents $\mathrm{Im}(\lambda)$, and the color represents the input phase angle θ. According to the

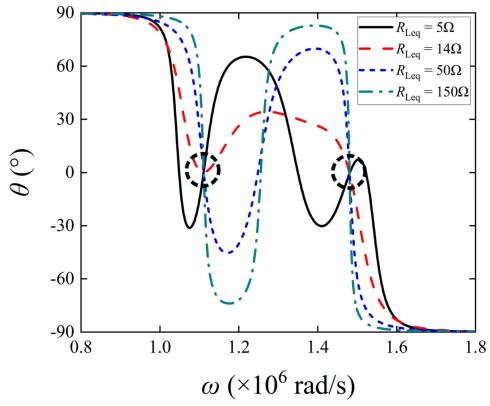

Fig. 6. Input phase angular θ versus the supply angular frequency ω of the 3-coil MC-WPT system.

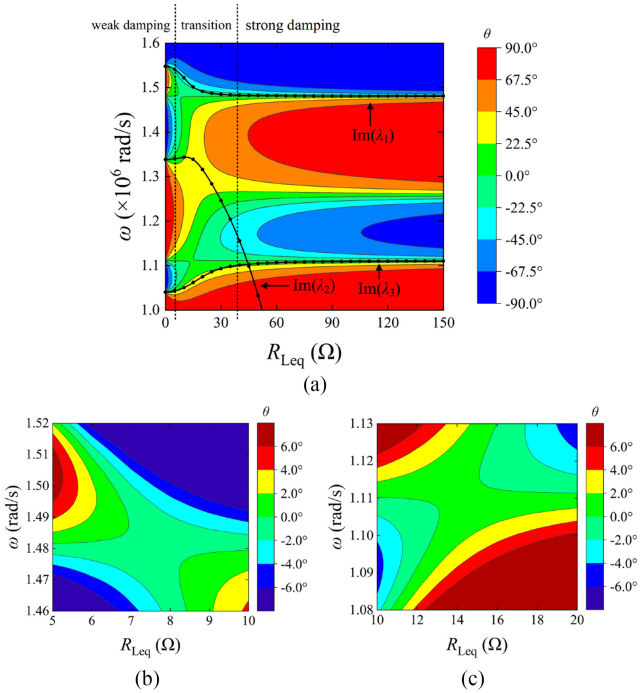

Fig. 7. Input-phase angular θ versus the supply angular frequency ω and equivalent load resistance $R_{\rm Leq}$ of the 3-coil MC-WPT system: (a) global; (b) partial details; and (c) partial details .

eigenvalues, the system can be divided into three stages: weak damping stage, transition stage, and strong damping stage.

a) When the system is in the weak damping stage, there are five zero-phase angle frequencies, and all eigenvalues slightly changes with $R_{\rm Leq}$. System characteristics are related to three eigenvalues.

b) When the system is in the transition stage, Re(λ_2) gradually increases. The number of eigenvalues that affect system characteristics gradually decreases from 3 to 2. Two zero-phase angle frequencies and one system resonant frequency may appear. When $R_{\rm Leq} = 14\ \Omega$, strictly speaking, there is only one zero-phase angle frequency. In most other cases, there are three zero-phase angle frequencies. From Figs. 5 and 7, during the transition stage, the changes of λ_1 and λ_3 are greater than those in the weak damping stage and the strong damping stage.

c) When the system is in the strong damping stage, there are always three zero-phase angular frequencies. λ_1 and λ_3 slightly changes with $R_{\rm Leq}$. System characteristics are only related to two eigenvalues.

The damping stage of the system can be judged according to the distribution of eigenvalues. The system is in strong damping stage when the real part of a certain eigenvalue is much larger than that of others. The system is in weak damping stage when there is not a large difference between the real parts of eigenvalues. In general, the system is in weak damping stage when the load resistance is very small, and the system is in strong damping stage when the load resistance is very large.

Within the global range of $R_{\rm Leq}$, there are at most five zero-phase angular frequencies, and at least only one zero-phase angular frequency. When ω is equal to 1.11×10^6 rad/s or 1.48×10^6 rad/s, the input phase angle θ is always zero except for some equivalent load resistance. From Fig. 6(b) and (c), in the cases, the input phase angle θ is below 2°, so it can be approximated as zero-phase angle frequency. 1.11×10^6 rad/s and 1.48×10^6 rad/s are fixed zero-phase angular frequencies in the global range of the equivalent load resistance, and they are equal to Im(λ_1) and Im(λ_3) in the strong damping stage, respectively.

The multirelay system can be designed according to actual engineering requirements. For example, the supply frequency can be slightly shifted up or down from the fixed zero-phase angular frequency to make the inverter output current lead or lag the supply voltage. The shifting direction depends on the system stage.

C. Constant Voltage/Current Frequencies

$U_{\rm out}$ represents the load voltage and $I_{\rm out}$ represents the load current. According to (27), $U_{\rm out}$ and $I_{\rm out}$ versus the supply angular frequency ω of the 3-coil MC-WPT system are plotted in Fig. 8. It can be seen that there are three constant voltages and two constant currents, and they are highlighted with dotted round frames. At these frequencies, the output voltage or output current with four equivalent load resistances remains constant.

In order to study the relationship between the eigenvalues and constant voltage/current characteristic with different load resistance, the output voltage $U_{\rm out}$ and the output current $I_{\rm out}$ versus the supply angular frequency ω and equivalent load resistance $R_{\rm Leq}$ of the 3-coil MC-WPT system is shown in Fig. 9 according to (16) and (27). The horizontal axis represents the equivalent load resistance $R_{\rm Leq}$, the vertical axis represents the supply angular frequency ω, the black dotted line represents Im(λ), and the color represents the output voltage $U_{\rm out}$ or the output current $I_{\rm out}$. When ω is equal to 1.04×10^6 rad/s, 1.34×10^6 rad/s, or 1.55×10^6 rad/s marked with arrows in Fig. 9(a), the output voltage remains almost constant. The three frequencies are equal to Im(λ_1), Im(λ_2), and Im(λ_3) with $R_{\rm Leq} = 0\ \Omega$. When ω is equal to 1.11×10^6 rad/s or 1.48×10^6 rad/s marked with arrows in Fig. 9(b), the output current remains almost constant.

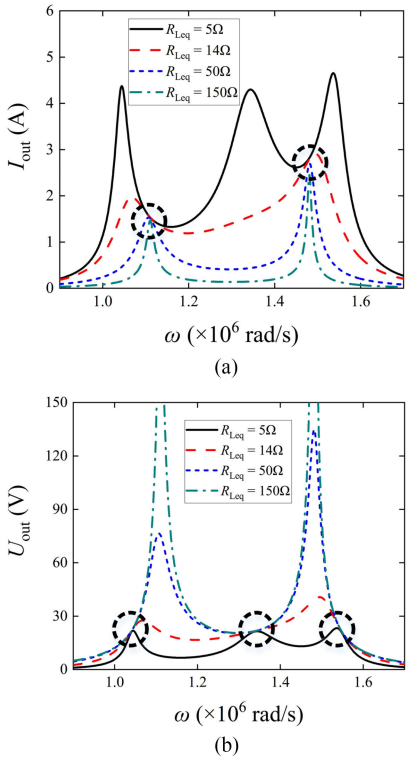

Fig. 8. Output voltage U_{out} and output current I_{out} versus the supply angular frequency ω in the 3-coil MC-WPT system. (a) Output current. (b) Output voltage .

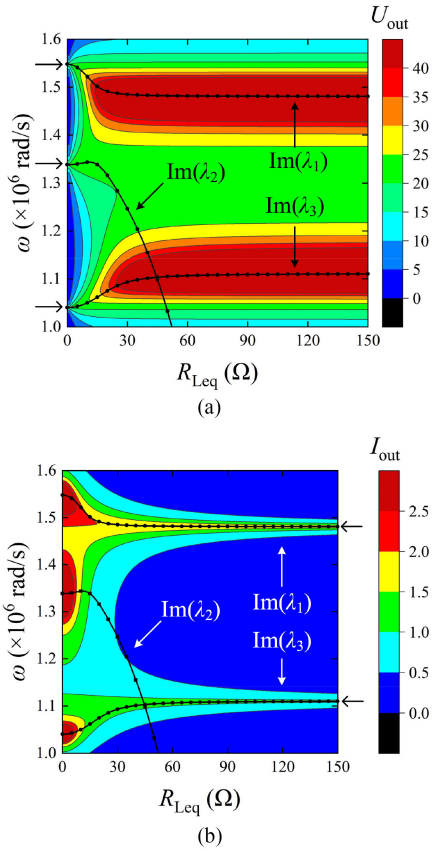

Fig. 9. Output voltage U_{out} and the output current I_{out} versus the supply angular frequency ω and equivalent load resistance R_{Leq} of the 3-coil MC-WPT system. (a) Output voltage. (b) Output current.

The two frequencies are equal to Im(λ_1) and Im(λ_3) in the strong damping stage.

D. Calculation Method of Key Frequencies

Let $\boldsymbol{R}_{\mathrm{w}}$ and $\boldsymbol{R}_{\mathrm{s}}$ represent matrix $\boldsymbol{R}$ of the system in the weak damping and the strong damping stages, respectively

$$\begin{cases} \mathbf{R}_{\mathrm{w}} = diag\left(R_1\ R_2\ \ldots\ R_{\mathrm{n}}\right) \\ \mathbf{R}_{\mathrm{s}} = diag\left(R_1\ R_2\ \ldots\ \infty\right) \end{cases} \tag{33}$$

$$\begin{cases} \mathbf{Q}_{\mathrm{w}}(\lambda) = \lambda^2\mathbf{L} + \lambda\mathbf{R}_{\mathrm{w}} + \mathbf{C} \\ \mathbf{Q}_{\mathrm{s}}(\lambda) = \lambda^2\mathbf{L} + \lambda\mathbf{R}_{\mathrm{s}} + \mathbf{C}. \end{cases} \tag{34}$$

$\boldsymbol{L}$ is nonsingular, let $\boldsymbol{A} - \lambda\boldsymbol{B}_{\mathrm{w}}$ is a linearization of $\boldsymbol{Q}_{\mathrm{w}}(\lambda)$, and let $\boldsymbol{A}$ - $\lambda\boldsymbol{B}_{\mathrm{s}}$ is a linearization of $\boldsymbol{Q}_{\mathrm{s}}(\lambda)$

$$\begin{cases} \mathbf{A} = \begin{bmatrix} \mathbf{C} & \mathbf{0} \\ \mathbf{0} & \mathbf{E} \end{bmatrix} \\ \mathbf{B}_{\mathrm{w}} = \begin{bmatrix} -\mathbf{R}_{\mathrm{w}} & -\mathbf{L} \\ \mathbf{0} & \mathbf{E} \end{bmatrix} \\ \mathbf{B}_{\mathrm{s}} = \begin{bmatrix} -\mathbf{R}_{\mathrm{s}} & -\mathbf{L} \\ \mathbf{0} & \mathbf{E} \end{bmatrix}. \end{cases} \tag{35}$$

By computing the generalized Schur decomposition, we obtain a numerically stable reduction. $\boldsymbol{S}$ and $\boldsymbol{T}$ are upper triangular and $\boldsymbol{W}$ and $\boldsymbol{Z}$ are unitary

$$\begin{cases} \mathbf{W}^*\mathbf{A}\mathbf{Z} = \mathbf{S}_{\mathrm{w}}, \quad \mathbf{W}^*\mathbf{B}_{\mathrm{w}}\mathbf{Z} = \mathbf{T}_{\mathrm{w}} \\ \mathbf{W}^*\mathbf{A}\mathbf{Z} = \mathbf{S}_{\mathrm{s}}, \quad \mathbf{W}^*\mathbf{B}_{\mathrm{s}}\mathbf{Z} = \mathbf{T}_{\mathrm{s}}. \end{cases} \tag{36}$$

$\Lambda(\mathbf{Q}_{\mathrm{w}})$and $\Lambda(\mathbf{Q}_{\mathrm{s}})$can be obtained from

$$\begin{cases} \Lambda\left(\mathbf{Q}_{\mathrm{w}}\right) = \left\{\frac{\mathbf{S}_{\mathrm{w}}(i,i)}{\mathbf{T}_{\mathrm{w}}(i,i)}\right\} \\ \Lambda\left(\mathbf{Q}_{\mathrm{s}}\right) = \left\{\frac{\mathbf{S}_{\mathrm{s}}(i,i)}{\mathbf{T}_{\mathrm{s}}(i,i)}\right\} \end{cases} \tag{37}$$

The expression of the three key frequencies are shown as (38) and (39). ω_{FZ}represents the fixed zero-phase angular frequency. ω_{CC} represents the constant current frequency and ω_{CV}represents the constant voltage frequency

$$\omega_{FZ}, \omega_{CC} = \mathrm{Im}\left(\Lambda\left(\mathbf{Q}_{\mathrm{s}}\right)\right) \tag{38}$$

$$\omega_{CV} = \mathrm{Im}\left(\Lambda\left(\mathbf{Q}_{\mathrm{w}}\right)\right). \tag{39}$$

Three coil system is taken as an example to discuss, but the analysis method is also suitable for two-coil and multicoil MC-WPT systems.

IV. Simulation and Experiment Verification

A. Simulation and Experimental Setup

A simulation model of the multirelay MC-WPT is built according Table I and Fig. 1. An experimental setup of multirelay MC-WPT system is built, as shown in Fig. 10, to verify the analysis method proposed in this article. The geometric parameters of the experimental setup are listed in Table III. The supply

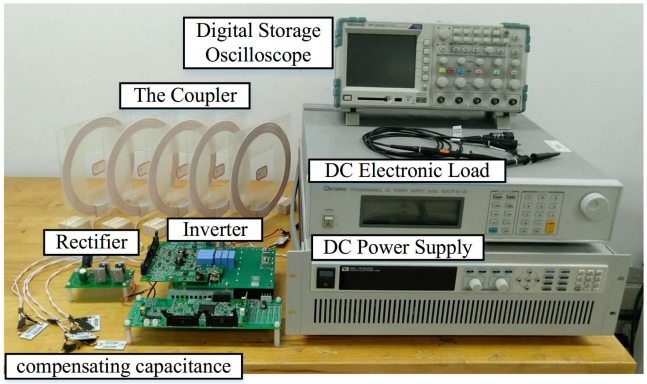

Fig. 10. Photograph of the experimental setup.

TABLE III
GEOMETRIC PARAMETERS OF THE EXPERIMENTAL SETUP

Parameter	Value	Parameter	Value
number of turns	10	transmission distance d	50 mm
layers of the coil	1	wire diameter	2 mm
radii of the coil	100 mm		

TABLE IV
COUPLER PARAMETERS OF THE EXPERIMENTAL SETUP

Parameter	Value
L_1, L_2, L_3, L_4, L_5	33.83 uH, 33.91 uH, 33.87 uH, 33.90 uH, 33.79 uH
C_1, C_2, C_3, C_4, C_5	18.76 nF, 18.61 nF, 18.77 nF, 18.68 nF, 18.78 nF
R_1, R_2, R_3, R_4, R_5	123 mΩ, 123 mΩ, 123 mΩ, 123 mΩ, 123 mΩ,
M_{12}, M_{13}, M_{14}, M_{15}	8.69 uH, 3.73 uH, 1.83 uH, 0.98 uH
M_{23}, M_{24}, M_{25}	8.97 uH, 3.79 uH, 1.80 uH,
M_{34}, M_{35}	8.93 uH, 3.66 uH
M_{45}	8.49 uH

voltage V is 24 V. The coupler parameters are listed in Table IV, which are measured with a LCR meter (IM3536).

B. Theoretical and Simulation Results

According to (28) and the simulation model, the simulation results and theoretical results of the impedance in 3-coil, 4-coil, and 5-coil MC-WPT system with $R_{\mathrm{L}} = 2\ \Omega$ are shown in Fig. 11. It is found that theoretical results and the simulation results are basically the same.

C. Theoretical and Experimental Results

1) Fixed Zero-Phase Angular Frequencies: According to (38), 1.12×10^6 , 1.05×10^6, and 1.01×10^6 rad/s are the fixed zero-phase angular frequencies of the 3-coil, 4-coil, and 5-coil MC-WPT system, respectively. The supply voltage and input current waveforms of the 3-coil, 4-coil, and 5-coil MC-WPT system are shown in Fig. 12. It can be found that there is almost no phase difference between supply voltage and input current.

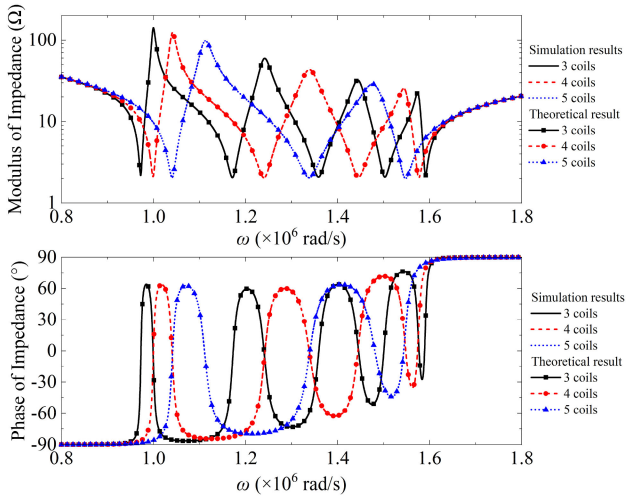

Fig. 11. Simulation results and theoretical results of the impedance in 3-coil, 4-coil, and 5-coil MC-WPT system with $R_{\mathrm{L}} = 2\ \Omega$.

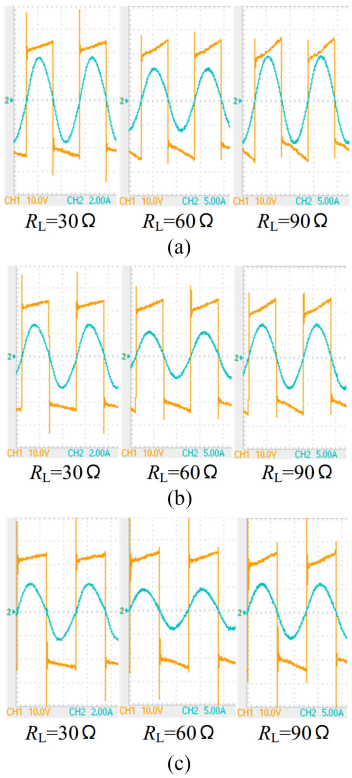

Fig. 12. Supply voltage and input current waveforms. (a) 3-coil MC-WPT system in 1.12×10^6 rad/s. (b) 4-coil MC-WPT system in 1.05×10^6 rad/s. (c) 5-coil MC-WPT system in 1.01×10^6 rad/s.

2) Constant Current/Voltage Frequencies: According to (38), 1.12×10^6, 1.05×10^6, and 1.01×10^6 rad/s are also the constant current angular frequencies of the 3-coil, 4-coil, and 5-coil MC-WPT system, respectively. The theoretical and measured output current I_{out} rms versus the load resistance R_{L} of the 3-coil system, 4-coil system, and 5-coil system are plotted in Fig. 13. The theoretical results are calculated with

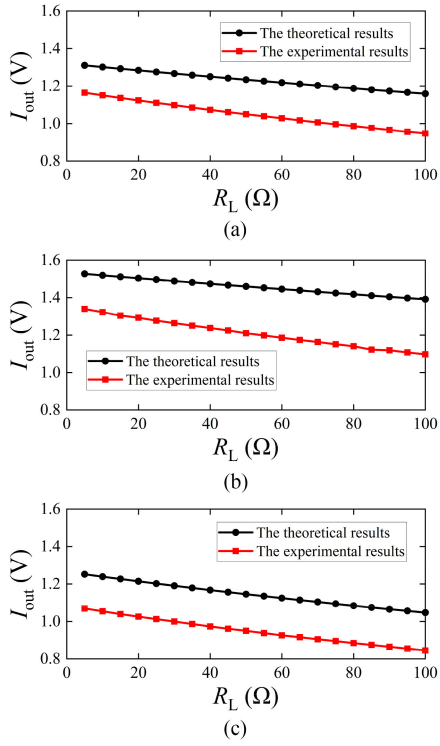

Fig. 13. Theoretical and measured output current $I_{\rm out}$ rms versus load resistance $R_{\rm L}$. (a) 3-coil MC-WPT system in 1.12×10^6 rad/s. (b) 4-coil MC-WPT system in 1.05×10^6 rad/s. (c) 5-coil MC-WPT system in 1.01×10^6 rad/s.

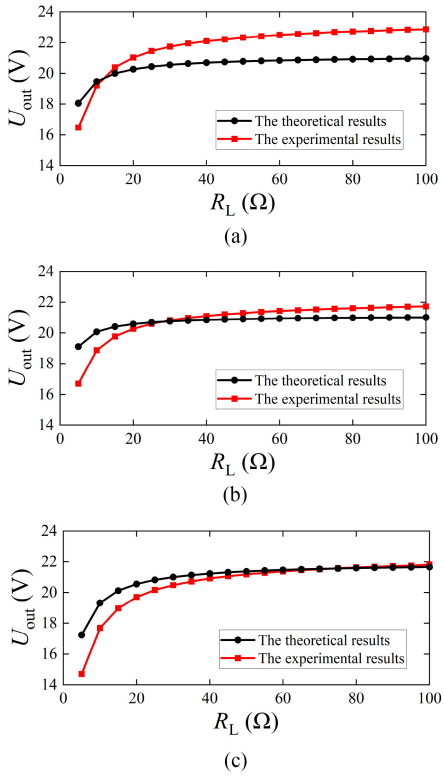

Fig. 14. Theoretical and measured output voltage $U_{\rm out}$ rms versus load resistance $R_{\rm L}$. (a) 3-coil MC-WPT system in 1.05×10^6 rad/s. (b) 4-coil MC-WPT system in 1.01×10^6 rad/s. (c) 5-coil MC-WPT system in 9.86×10^5 rad/s.

the experimental setup parameters. The result shows that the multirelay MC-WPT systems all has good constant current output characteristics. The average current change rates of 3-coil, 4-coil, and 5-coil MC-WPT system are 2.5×10^{-3}, 2.3×10^{-3}, and 2.4×10^{-3} A/Ω, respectively.

According to (39), 1.05×10^6, 1.01×10^6, and 9.86×10^5 rad/s are the constant voltage angular frequencies of the 3-coil, 4-coil, and 5-coil MC-WPT system, respectively. The theoretical and measured output voltage $U_{\rm out}$ rms versus the load resistance $R_{\rm L}$ of the 3-coil system, 4-coil system, and 5-coil system are plotted in Fig. 14. The theoretical results are also calculated with the experimental setup parameters. It can be seen from Fig. 13 that the multirelay MC-WPT systems all has good constant voltage output characteristics. The average voltage change rates of 3-coil, 4-coil, and 5-coil MC-WPT system are 6.3×10^{-2}, 6.3×10^{-2}, 6.3×10^{-2} V/Ω, respectively.

There are some deviations between the theoretical results and the measured results, which is mainly caused by the measuring error of electrical parameters and power losses of the inverter and the rectifier.

D. Relationship Between System Output and Number of Coils

Theoretical calculation results of the system output with simulation parameters are shown as Table V. $R_{\rm Leq}$ is equal to 50 Ω. It can be found that output current decreases when the number of coils increases in constant current frequencies, and the output voltage is the nearly the same as each other. Constant current frequencies of 4-coil MC-WPT system are equal to the constant voltage frequencies of 3-coil MC-WPT system. Constant current frequencies of 5-coil MC-WPT system are equal to the constant voltage frequencies of 4-coil MC-WPT system.

TABLE V
THEORETICAL CALCULATION RESULTS OF THE SYSTEM OUTPUT IN CONSTANT CURRENT/VOLTAGE FREQUENCIES

n	3		4		5	
	$\omega(\times10^6)$	RMS	$\omega(\times10^6)$	RMS	$\omega(\times10^6)$	RMS
$I_{\rm out}$	1.11	1.5276	1.04	1.3284	1.00	1.2142
	1.48	2.6993	1.34	2.2107	1.24	1.8951
			1.55	2.6817	1.45	2.4708
					1.58	2.4705
$U_{\rm out}$	1.04	21.4603	1.00	21.5196	0.97	21.3568
	1.34	21.5641	1.24	21.5524	1.17	21.4399
	1.55	21.8635	1.45	21.6066	1.36	21.5845
			1.58	21.1580	1.50	21.4970
					1.59	21.6277

The comparison of calculation results with experimental parameters and experimental results is shown as Table VI. Equivalent load resistance $R_{\rm L}$ is equal to 50 Ω. Operating frequencies are 1.05×10^6, 1.01×10^6, and 9.86×10^5 rad/s, respectively. It can be seen that the experimental results agree with the theoretical analysis.

TABLE VI
COMPARISON OF THEORETICAL AND EXPERIMENTAL RESULTS

Numbers of coils	3		4		5	
	I_{out}	U_{out}	I_{out}	U_{out}	I_{out}	U_{out}
Calculation results with experimental parameters	1.46	20.90	1.23	20.78	1.15	21.37
Experimental result	1.21	21.29	1.05	22.33	0.95	21.18

V. CONCLUSION

In this article, an analysis method based on QEP for the multirelay MC-WPT system has been proposed. The contributions are as follows.

1) The analysis method was proven to be capable of getting the solution of key frequencies including zero-phase frequencies and constant current/voltage frequencies.
2) As the order of the system increases, the analysis process will not become more complicated.
3) Fixed zero-phase angular frequencies and the constant current operating frequencies are equal to the imaginary parts of the eigenvalues in the weak damping stage, and the constant voltage operating frequencies are equal to the imaginary parts of the complex eigenvalues in the strong damping stage.

The simulation model and the experimental setup are built. The calculated results of the induced current are consistent with the simulation results. The results show that theoretical results of fixed zero-phase angular frequency and the constant current/voltage frequency are consistent with experimental results. Therefore, the feasibility and effectiveness of this analysis method were verified. The analysis method provided in this work is helpful for the application of multirelay MC-WPT systems.

REFERENCES

[1] B. H. Waters, A. P. Sample, P. Bonde, and J. R. Smith, "Powering a ventricular assist device (VAD) with the free-range resonant electrical energy delivery (FREE-D) system," *Proc. IEEE*, vol. 100, no. 1, pp. 138–149, Jan. 2012.

[2] A. K. RamRakhyani and G. Lazzi, "Multicoil telemetry system for compensation of coil misalignment effects in implantable systems," *IEEE Antennas Wireless Propag. Lett.*, vol. 11, pp. 1675–1678, 2012.

[3] M. Fareq *et al.*, "Solar wireless power transfer using inductive coupling for mobile phone charger," in *Proc. IEEE 8th Int. Power Eng. Optim. Conf.*, Langkawi, Malaysia, 2014, pp. 473–476.

[4] B. Esteban, M. Sid-Ahmed, and N. C. Kar, "A comparative study of power supply architectures in wireless EV charging systems," *IEEE Trans. Power Electron.*, vol. 30, no. 11, pp. 6408–6422, Nov. 2015.

[5] J.-Y. Lee and B.-M. Han, "A bidirectional wireless power transfer EV charger using self-resonant PWM," *IEEE Trans. Power Electron.*, vol. 30, no. 4, pp. 1784–1787, Apr. 2015.

[6] S. Y. R. Hui, W. Zhong, and C. K. Lee, "A critical review of recent progress in mid-range wireless power transfer," *IEEE Trans. Power Electron.*, vol. 29, no. 9, pp. 4500–4511, Sep. 2014.

[7] Y. Li *et al.*, "Reconfigurable intermediate resonant circuit based WPT system with load-independent constant output current and voltage for charging battery," *IEEE Trans. Power Electron.*, vol. 34, no. 3, pp. 1988–1992, Mar. 2019.

[8] W. Q. Niu, W. Gu, J. X. Chu, and A. D. Shen, "Coupled-mode analysis of frequency splitting phenomena in CPT systems," *Electron. Lett.*, vol. 48, no. 12, pp. 723–724, Jun. 2012.

[9] M. Ettorre and A. Grbic, "A transponder-based, nonradiative wireless power transfer," *IEEE Antennas Wireless Propag. Lett.*, vol. 11, pp. 1150–1153, 2012.

[10] A. Kurs, A. Karalis, R. Moffatt, J. D. Joannopoulos, and M. Soljacic, "Wireless power transfer via strongly coupled magnetic resonances," *Science*, vol. 317, no. 5834, pp. 83–86, 2007.

[11] H. Li, K. Wang, L. Huang, W. Chen, and X. Yang, "Dynamic modeling based on coupled modes for wireless power transfer systems," *IEEE Trans. Power Electron.*, vol. 30, no. 11, pp. 6245–6253, Nov. 2015.

[12] N. Ali, Z. Liu, Y. Hou, H. Armghan, X. Wei, and A. Armghan, "LCC-S based discrete fast terminal sliding mode controller for efficient charging through wireless power transfer," *Energies*, vol. 13, no. 6, pp. 1–18, 2020.

[13] C. K. Lee, W. X. Zhong, and S. Y. R. Hui, "Effects of magnetic coupling of nonadjacent resonators on wireless power domino-resonator systems," *IEEE Trans. Power Electron.*, vol. 27, no. 4, pp. 1905–1916, Apr. 2012.

[14] C. Zhang, D. Lin, N. Tang, and S. Y. Ron Hui, "A novel electric insulation string structure with high-voltage insulation and wireless power transfer capabilities," *IEEE Trans. Power Electron.*, vol. 33, no. 1, pp. 87–96, Jan. 2018.

[15] B. H. Waters, B. J. Mahoney, V. Ranganathan, and J. R. Smith, "Power delivery and leakage field control using an adaptive phased array wireless power system," *IEEE Trans. Power Electron.*, vol. 30, no. 11, pp. 6298–6309, Nov. 2015.

[16] D. Ahn and S. Hong, "A study on magnetic field repeater in wireless power transfer," *IEEE Trans. Ind. Electron.*, vol. 60, no. 1, pp. 360–371, Jan. 2013.

[17] Y. Sun, Z.-J. Liao, Z.-H. Ye, C.-S. Tang, and P.-Y. Wang, "Determining the maximum power transfer points for MC-WPT systems with arbitrary number of coils," *IEEE Trans. Power Electron.*, vol. 33, no. 11, pp. 9734–9743, Nov. 2018.

[18] C. Cheng, W. Li, Z. Zhou, Z. Deng, and C. Mi, "A load-independent wireless power transfer system with multiple constant voltage outputs," *IEEE Trans. Power Electron.*, vol. 35, no. 4, pp. 3328–3331, Apr. 2020.

[19] Y. Wang, Y. Yao, X. Liu, and D. Xu, "Analysis on S/CLC compensation topology for wireless power transfer," *Diangong Jishu Xuebao/Trans. China Electrotechnical Soc.*, vol. 32, no. 22, pp. 34–41, 2017.

[20] M. Fu, C. Ma, and X. Zhu, "A cascaded boost-buck converter for high-efficiency wireless power transfer systems," *IEEE Trans. Ind. Inform.*, vol. 10, no. 3, pp. 1972–1980, Aug. 2014.

[21] K. Colak, E. Asa, M. Bojarski, D. Czarkowski, and O. C. Onar, "A novel phase-shift control of semibridgeless active rectifier for wireless power transfer," *IEEE Trans. Power Electron.*, vol. 30, no. 11, pp. 6288–6297, Nov. 2015.

[22] Z. Dong, S. Liu, X. Li, Z. Xu, and L. Yang, "A novel long-distance wireless power transfer system with constant current output based on domino-resonator," *IEEE J. Emerg. Sel. Topics Power Electron.*, doi: 10.1109/JESTPE.2020.2983231

[23] F. Tisseur and K. Meerbergen, "The quadratic eigenvalue problem," (in English), *SIAM Rev.*, vol. 43, no. 2, pp. 235–286, Jun. 2001.

[24] Z.-J. Liao, Y. Sun, Z.-H. Ye, C.-S. Tang, and P.-Y. Wang, "Resonant analysis of magnetic coupling wireless power transfer systems," *IEEE Trans. Power Electron.*, vol. 34, no. 6, pp. 5513–5523, Jun. 2019.

[25] S. Raju, R. Wu, M. Chan, and C. P. Yue, "Modeling of mutual coupling between planar inductors in wireless power applications," *IEEE Trans. Power Electron.*, vol. 29, no. 1, pp. 481–490, Jan. 2014.

[26] F. Tisseur, "Structured pseudospectra for polynomial eigenvalue problems, with applications," *SIAM J. Matrix Anal. Appl.*, vol. 23, pp. 187–208, 2001.

Xinyu Hou received the B.E. degree in 2017 from the College of Automation, Chongqing University, Chongqing, China, where he is currently working toward the Ph.D. degree in control theory and control engineering.

His research interests include wireless power transfer and power electronics.

Yugang Su (Member, IEEE) received the B.E. and M.E. degrees in industry automation and the Ph.D. degree in control theory and control engineering from Chongqing University, Chongqing, China, in 1985, 1993, and 2004, respectively.

From 2008 to 2009, he was a Visiting Scholar with the University of Queensland, Brisbane, Australia. He is currently a Professor with the College of Automation, Chongqing University. His research interests include power electronics, control theory and applications, wireless power transfer.

Zhiping Zuo was born in Chongqing, China, in 1989. He received the B.E. degree from the School of Electrical and Electronic Engineering, Huazhong University of Science and Technology, Wuhan, China, in 2012, and the Ph.D. degree from the School of Electrical Engineering, Chongqing University, Chongqing, China.

His current research interests include the fabrication of anti-icing materials application on insulators and wireless power transfer.

Xin Dai (Member, IEEE) received the B.S. degree in industrial automation from Chongqing Technology and Business University (formerly Yuzhou University), Chongqing, China, in 2000, and the Ph.D. degree in control theory and control engineering from the School of Automation, Chongqing University, Chongqing, China, in 2006.

In 2012, he was a Visiting Scholar with The University of Auckland, New Zealand. He is currently a Professor with the School of Automation, Chongqing University, Chongqing, China. His current research interests include inductive power transfer technology and nonlinear dynamic behavior analysis of power electronics.

Yingjun Fei received the B.E. degree in 2018 from the College of Automation, Chongqing University, Chongqing, China, where he is currently working toward the Ph.D. degree in control theory and control engineering.

His research interests include wireless power transfer and power electronics.